

be attributed to a higher peak electric field near the drain junction, which increases with increasing tilt angle.

IV. CONCLUSIONS

The experimental results presented in this paper show optimization trends for SH p-MOSFETs with various halo implantation angles. As can be seen from the experimental data, SH MOSFETs show a higher current drive and saturation transconductance, which can be attributed to an increase in the average velocity of channel carriers in these devices. It has also been shown that a decrease in the peak lateral electric field in the SH MOSFETs gives rise to an improved reliability performance, as can be seen from the measured substrate currents and interface degradation. Our results also indicate that the lower tilt angles for V_T adjust implant give rise to a better confinement of channel doping concentration near the source side, which is effective in improving the device transconductance as well as the reliability performance.

REFERENCES

- [1] T. Buti, S. Ogura, N. Rovedo, and K. Tobomatsu, "A new asymmetrical halo source GOLD drain (HS-GOLD) sub half micrometer n-MOSFET design for reliability and performance," *IEEE Trans. Electron Devices*, vol. 38, pp. 1757–1764, Aug. 1991.
- [2] C. C. Shen, J. Muruguia, N. Goldsman, M. Peckerar, J. Melngailis, and D. Antoniadis, "Using focused ion beam to optimize sub micron MOSFET characteristics," *IEEE Trans. Electron Devices*, vol. 45, p. 453, Feb. 1998.
- [3] J. P. John, V. Ilderem, C. Park, J. Teplik, K. Klein, and S. Chen, "A low voltage graded-channel MOSFET (LV-GCMOS) for sub 1-volt micro-controller application," in *VLSI Tech. Dig.*, 1999, pp. 178–179.
- [4] B. Cheng, V. Ramgopal Rao, B. Ikegami, and J. C. S. Woo, "Realization of sub 100nm asymmetric channel MOSFETs with excellent short channel performance and reliability," in *ESSDERC Tech. Dig.*, Bordeaux, France, 1998, pp. 520–523.
- [5] B. Cheng, A. Inani, V. Ramgopal Rao, and J. C. S. Woo, "Channel engineering for high speed sub-1.0 V power supply deep sub-micron CMOS," in *VLSI Tech. Dig.*, Kyoto, Japan, June 1999, pp. 79–80.
- [6] S. Mahapatra, V. Ramgopal Rao, C. D. Parikh, J. Vasi, B. Cheng, and J. C. S. Woo, "A study of 100nm channel length asymmetric MOSFETs by using charge pumping," in *11th Biennial Conf. Insulating Films on Semiconductors*, Koster Banz, Germany, June 16–19, 1999.
- [7] B. Cheng, V. Ramgopal Rao, and J. C. S. Woo, "Exploration of velocity overshoot in a high-performance deep sub 100 nm SOI MOSFET with asymmetric channel profile," *IEEE Electron Device Lett.*, vol. 20, pp. 538–540, Oct. 1999.
- [8] Avanti TCAD Tools: Suprem 4 Process Simulator, San Jose, CA, 1999.
- [9] S. Mahapatra, V. Ramgopal Rao, C. D. Parikh, J. Vasi, B. Cheng, and J. C. S. Woo, "A study of 100nm channel length asymmetric MOSFETs by using charge pumping," *Microelectron. Eng.*, vol. 48, no. 1–4, pp. 193–196, Sept. 1999.

New Collector Undercut Technique Using a SiN Sidewall for Low Base Contact Resistance in InP/InGaAs SHBTs

Kyungho Lee, Daekyu Yu, Minchul Chung, Jongchan Kang, and Bumman Kim

Abstract—A new collector undercut process using SiN protection sidewall has been developed for high speed InP/InGaAs single heterojunction bipolar transistors (HBTs). The HBTs fabricated using the technique have a larger base contact area, resulting in a smaller DC current gain and smaller base contact resistance than HBTs fabricated using a conventional undercut process while maintaining low C_{bc} . Due to the reduced base contact resistance, the maximum oscillation frequency (f_{max}) has been enhanced from 162 GHz to 208 GHz. This result clearly shows the effectiveness of this technique for high-speed HBT process, especially for the HBTs with a thick collector layer, and narrow base metal width.

Index Terms—Base-collector capacitance, base resistance, collector undercut, heterojunction bipolar transistors (HBTs).

I. INTRODUCTION

Many research works have been devoted to reducing the base-collector capacitance (C_{bc}) and base resistance (R_b) in HBT for a high speed operation since $f_{max} = \sqrt{f_T/8\pi R_b C_{bc}}$. Ion implantation technique is the most widely used for reduced C_{bc} of GaAs HBTs, but it is not a viable technique for InP-based HBTs [1], [2]. Regrown base [3], and L-shaped base electrodes [4] are used for reduction of R_b . The transferred substrate technique, which can minimize the C_{bc} , yields an HBT with f_{max} in excess of 1 THz [5]. Simple collector undercut is the most widely used to reduce the C_{bc} of InP double-HBTs due to the selective etching nature [6]–[8]. In the case of single-HBTs, however, the base layer is also etched during the collector undercut process because the selective etch cannot be employed.

In this brief, we propose a new collector undercut technique that does not etch the base layer laterally using SiN protection sidewall. Because the base contact layer is intact during the undercut, the contact resistance is maintained low. In this process, the surfaces of the emitter sidewall and extrinsic base are passivated by polyimide [9] and a low parasitic interconnection using air-bridge is also employed. The RF performance data of the HBT clearly demonstrate the effectiveness of the new process technique.

II. DEVICE STRUCTURE AND FABRICATION

The epitaxial layer of the fabricated HBTs is grown by solid source molecular beam epitaxy (SSMBE) on a Fe-doped semi-insulating (100) InP substrate, starting with a 5000 Å InGaAs subcollector layer and 6000-Å-thick, $2.0 \times 10^{16} \text{ cm}^{-3}$ Si-doped collector layer. The 600 Å InGaAs base is Be-doped to $3.0 \times 10^{19} \text{ cm}^{-3}$ with a 70-Å undoped spacer. The emitter layer is a 1000-Å InP with Si-doped to $5.0 \times 10^{17} \text{ cm}^{-3}$, followed by the InGaAs cap layer. The details are outlined in Table I.

Fabrication starts with the evaporation of Ti/Pt/Au emitter contact metals. Emitter etch, which is the most delicate step, was carried out by

Manuscript received October 15, 2001; revised January 22, 2002. This work was supported in part by the Agency for Defense Development, the BK-21 Project of the Ministry of Education, and the Ministry of Commerce, Industry, and Energy. The review of this brief was arranged by K. M. Lau.

The authors are with the Department of Electronic and Electrical Engineering and Microwave Application Research Center, Pohang University of Science and Technology, Pohang, Kyungbuk, 790-784 Korea (e-mail: bmkim@postech.ac.kr).

Publisher Item Identifier S 0018-9383(02)04881-5.

TABLE I
EPITAXIAL LAYER STRUCTURE OF FABRICATED HBTs

Layer	Composition & Carrier type	Doping (cm^{-3})	Thickness (\AA)
Emitter-cap	n-InGaAs	5×10^{19}	800
	n-InP	1×10^{19}	600
	n-InP	2×10^{18}	600
Emitter	n-InP	5×10^{17}	1000
Spacer	i-InGaAs	undoped	70
Base	p-InGaAs	3×10^{19}	600
Collector	n-InGaAs	2×10^{16}	6000
Etch-stop	n-InP	1×10^{19}	50
Subcollector	n-InGaAs	5×10^{19}	5000

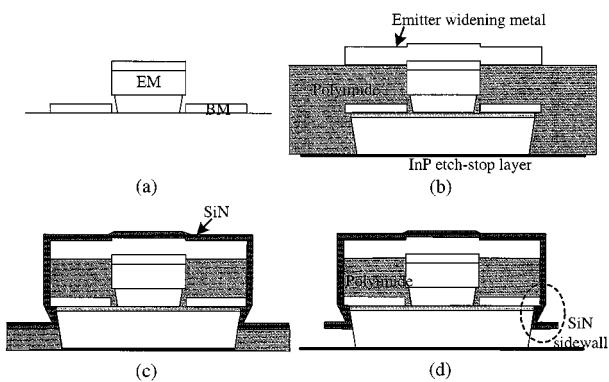


Fig. 1. Process flow of new collector undercut technique. (a) Self-aligned base metal, (b) emitter metal widening, (c) SiN deposition, and (d) removal of residual polyimide.

selective etch of citric-based and subsequent hydrochloric-based wet processes, and the emitter was slightly undercut. After the emitter etch, a self-aligned Pt/Ti/Pt/Au base metal was evaporated [Fig. 1(a)]. The emitter was protected by photoresist using base contact mask, and the base and collector layers were then etched with a citric-based etchant. Next, polyimide was coated and then flatly etched without mask using O_2 RIE until the emitter metal was exposed. Next, a Ti/Au emitter widening metal was evaporated [Fig. 1(b)], and second, polyimide etch was performed until the thickness of the residual polyimide was about 2000 \AA . Next, SiN was deposited [Fig. 1(c)]. The SiN was mask etched and the residual polyimide was removed by ashing [Fig. 1(d)]. The collector was undercut but the base layer was protected by the SiN sidewall. A sulfuric-acid based etchant was used. The subcollector was etched for isolation, and AuGe/Ni/Au collector ohmic metal and pad metal were evaporated and alloyed. Au air-bridge formation followed. For comparison, conventionally processed HBTs were also built. We call the former HBT-N and the latter HBT-C. The schematic cross sections, which are not accurately scaled, of both devices used for evaluations are shown in Fig. 2(a) and (b). An SEM picture of the fabricated HBT with new collector undercut process is shown in Fig. 3. For high speed InP HBTs, the emitter and base metal widths are 1 μm . The base-to-emitter spacing measured from SEM picture is 0.1 μm . The

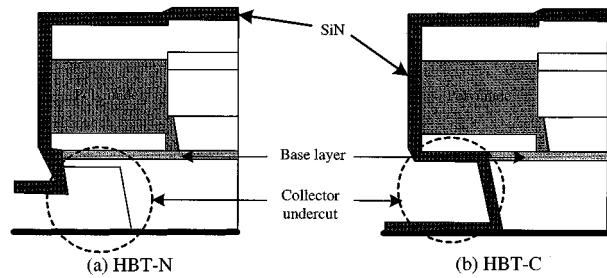


Fig. 2. Schematic cross sections of fabricated devices: (a) HBT-N with new undercut process and (b) HBT-C with conventional undercut process.

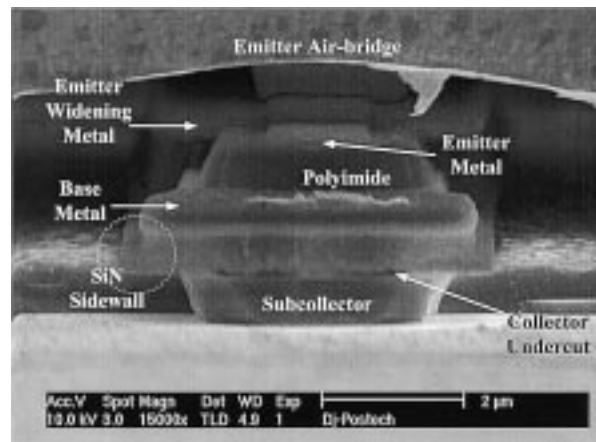


Fig. 3. SEM picture of the front view of the fabricated HBT with new undercut process.

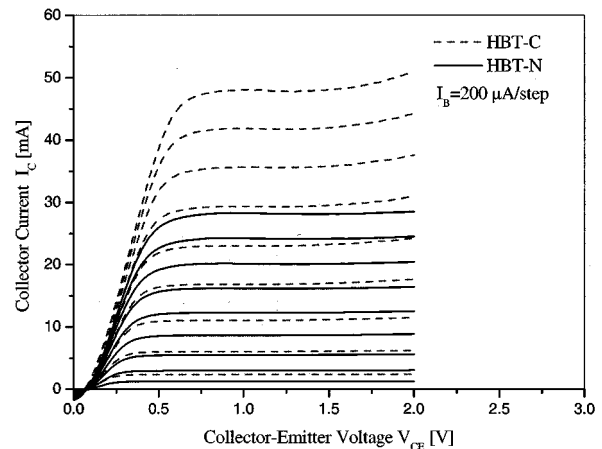


Fig. 4. Common emitter $I_C - V_{CE}$ characteristics of HBT-C (dashed lines) and HBT-N (solid lines).

thickness of the collector layer is 0.6 μm with 0.5 μm subcollector. During the collector undercut of more than 0.6 μm , if the base layer is not protected it can be easily attacked.

III. RESULTS AND DISCUSSION

The current-voltage ($I-V$) curves of the two HBTs with $1 \times 20 \mu\text{m}^2$ emitter area were measured and depicted in Fig. 4. As shown, the common-emitter dc current gain (β) of the HBTs are about 23 and 14

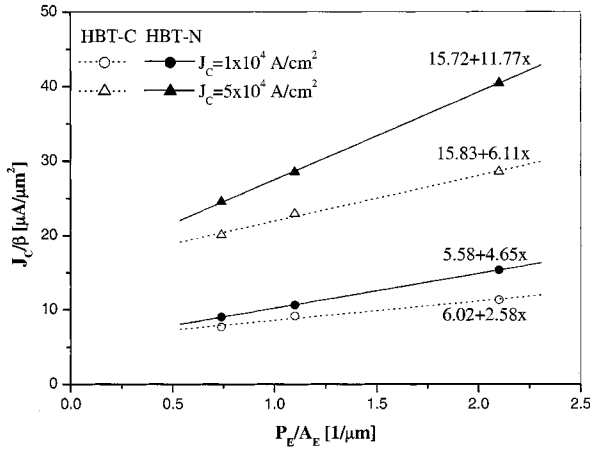


Fig. 5. J_C/β versus P_E/A_E characteristics for HBT-C (empty) and HBT-N (filled) at $J_C = 1 \times 10^4$ A/cm² and $J_C = 5 \times 10^4$ A/cm². Emitter sizes used: 1×20 μm², 2×20 μm², and 3×20 μm².

for HBT-C and HBT-N, respectively, at a collector current density of 1×10^5 A/cm². In order to explain the difference of dc current gains of the devices, the base currents were decomposed using the following relationship:

$$J_C \frac{1}{\beta} = J_{BA} + 2J_{BP} \left(\frac{1}{W_E} + \frac{1}{L_E} \right) \quad (1)$$

where J_{BA} is the base current component including bulk recombination, space charge recombination, and back injection currents, which are proportional to the emitter area, J_{BP} is the base current component including surface recombination and contact recombination currents, which are proportional to the emitter periphery. J_C/β was measured as a function of P_E/A_E and is depicted in Fig. 5. From the figure, we found J_{BA} of 15.72 μA/μm² and 15.83 μA/μm² and J_{BP} of 6.11 μA/μm and 11.77 μA/μm at a collector current density of 5×10^4 A/cm² for HBT-C and HBT-N, respectively. These strong emitter size effect arose from the contact and surface recombination currents due to small emitter width and narrow base-emitter contact spacing, although InP-based HBTs have low surface recombination velocity and launcher effect by emitter-base hetero-interface. Since both devices were made with the same wafer and the same process, except the undercut collector step, the two devices are identical except the undercut area. As shown in Fig. 2, HBT-N has a large base contact area compared to HBT-C. Therefore, it has a larger contact recombination current. Moreover, the large unpassivated area below the base layer further enhances the surface recombination for HBT-N. Therefore, it has a lower β . The breakdown voltages of each device at an open base BV_{ceo} are 15 V for the HBT-C and 17 V for the HBT-N at a collector current of 100 μA. As shown in I - V curves, the knee voltage and offset voltage are 0.36 V and 0.37 V at a collector current density of 1×10^5 A/cm², 0.08 V and 0.09 V for HBT-C and HBT-N, respectively. These differences in dc characteristics arise from difference of the dc current gain.

Microwave S -parameters were measured on wafer over a frequency range of 0.5 to 40 GHz using an HP8510C network analyzer. Fig. 6 shows a comparison of gain-frequency characteristics of the HBT-C and HBT-N. The f_T and f_{max} of HBT-C are 78 GHz and 162 GHz, respectively, at $I_C = 14.3$ mA and $V_{CE} = 2.0$ V, and those of HBT-N are 80 GHz and 208 GHz, respectively, at the same bias point. HBT-C is more stable than HBT-N. Fig. 7 shows the dependencies of f_T and f_{max} on the collector current density for both devices, which are quite similar. These differences in characteristics can be described by the differences in base resistance R_b , since a device can be more stable

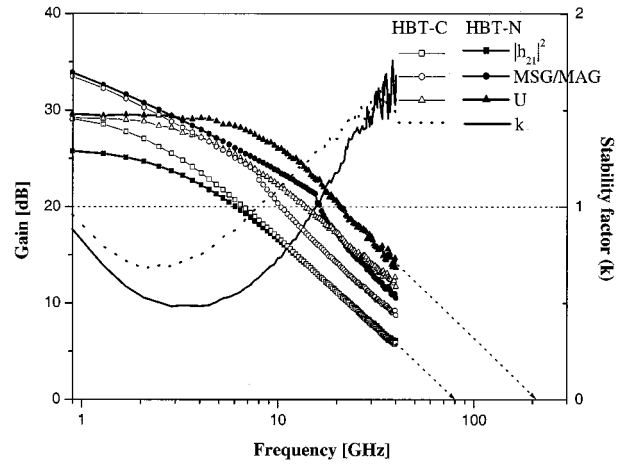


Fig. 6. Frequency dependencies of $|h_{21}|^2$, MSG/MAG, U, and stability factor (k) as determined by S -parameter measurements.

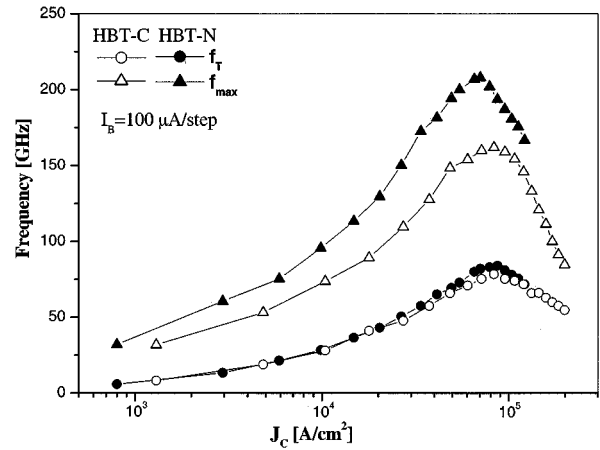


Fig. 7. Dependence of f_T and f_{max} on collector current density for HBT-C and HBT-N at $V_{CE} = 2.0$ V.

for larger R_b and f_{max} is dependent on R_b , also. Therefore, we have investigated R_b , which is given by

$$R_b = \frac{R_{SB}S_E}{12L_E} + \frac{R_{SB}S_{EB}}{2L_E} + \frac{\sqrt{\rho_{BC}R_{SB}}}{2L_B} \coth S_B \sqrt{\frac{R_{SB}}{\rho_{BC}}} \quad (2)$$

where R_{SB} is base sheet resistance, S_E and S_B are emitter and base widths (1.0 μm in our case), L_E and L_B are emitter and base lengths, respectively, S_{EB} is emitter to base spacing (0.1 μm), and ρ_{BC} is base-specific contact resistivity. Base sheet resistance of 640 Ω/□ and specific contact resistivity of 3.0×10^{-6} Ω·cm² were measured using transmission line measurement pattern. The transfer length, L_T , expressed as $\sqrt{\rho_{BC}/R_{SB}}$ is 0.68 μm for our case, and it can be longer for the smaller base sheet resistance and larger base specific contact resistivity. As shown in Fig. 2(b), the effective base contact width becomes narrower for HBT-C due to the lateral etch of the base layer. R_b of the device can be increased exponentially as the base contact area becomes narrower than L_T [see the last term of (2)]. Thus, R_b of the HBT-C can be large. Since the base contact layer of HBT-N is maintained intact during the collector undercut formation, it is expected that the R_b of HBT-N will be lower.

To estimate the total base resistance R_b , the small signal model parameters of the two HBTs were extracted and listed in Table II. As shown, both devices have similar values of C_{bc} , indicating that the capacitances are reduced successfully for both devices. However, the base resistances are quite different, 31.53 Ω and 20.40 Ω for HBT-C

TABLE II
EXTRACTED SMALL-SIGNAL PARAMETERS OF THE TWO HBTs
WITH $1 \times 20 \mu\text{m}^2$ EMITTER AREA

	R_E	R_B	g_m	r_π	C_π	C_{bc}	C_{bcx}
	(Ω)	(Ω)	(mS)	(Ω)	(pF)	(fF)	(fF)
HBT-C	1.38	31.53	552	48.3	1.14	3.15	10.82
HBT-N	1.42	20.40	544	40.1	1.05	3.04	10.94

and HBT-N, respectively. This data clearly shows that the new process with SiN protection wall is working properly. Consequently, the base resistance, R_b , is reduced by 35% and maximum oscillation frequency, f_{max} , is enhanced by 30% (from 162 GHz to 208 GHz). Since the base resistance does not affect the transit time, f_{TS} of the two HBTs are quite similar, around 80 GHz.

IV. CONCLUSION

In order to reduce C_{bc} without increasing R_b , we have developed a new collector undercut process using a SiN protection sidewall. Since the base layer is intact during the collector undercut formation, it maintained a wide base contact region, while the region for conventional process is laterally etched. Due to the wide base contact region, the HBTs have a smaller current gain and smaller base resistance with similarly low C_{bc} compared to the HBTs with the conventional undercut process. We have demonstrated a 35% reduction of base resistance and a 30% increase of f_{max} . f_{max} is enhanced from 162 GHz to 208 GHz for $1 \times 20 \mu\text{m}^2$ emitter HBTs.

ACKNOWLEDGMENT

The authors would like to thank M. S. Kim and J. H. Shin, LG Electronics Institute of Technology, Seoul, Korea, for their help with the e-beam metallization process.

REFERENCES

- [1] H.-F. Chau and Y.-C. Kao, "High f_{max} InAlAs/InGaAs heterojunction bipolar transistors," in *IEDM Tech. Dig.*, 1993, pp. 783–786.
- [2] M.-C. Ho, R. A. Johnson, W. J. Ho, M. F. Chang, and P. M. Asbeck, "High-performance low-base-collector capacitance AlGaAs/GaAs heterojunction bipolar transistors fabricated by deep ion implantation," *IEEE Electron Device Lett.*, vol. 16, pp. 512–514, Nov. 1995.
- [3] H. Shimawaki, Y. Amamiya, N. Furuhashi, and K. Honjo, "High- f_{max} AlGaAs/InGaAs and AlGaAs/GaAs HBTs with p+/p regrown base contacts," *IEEE Trans. Electron Devices*, vol. 42, pp. 1735–1744, Oct. 1995.
- [4] M. Yanagihara, H. Sakai, Y. Ota, M. Tanabe, K. Inoue, and A. Tamura, "253-GHz f_{max} AlGaAs/GaAs HBT with Ni/Ti/Pt/Ti/Pt-contact and L-shaped base electrode," in *IEDM Tech. Dig.*, 1990, pp. 807–810.
- [5] M. Rodwell, Y. Betsler, S. Jaganathan, T. Mathew, P. K. Sundararajan, S. C. Martin, R. P. Smith, Y. Wei, M. Urteaga, D. Scott, and S. Long, "Submicron lateral scaling of HBTs and other vertical-transport devices: Toward THz bandwidths," in *Proc. GaAs 2000 Conf.*, Paris, France, Oct. 2000, pp. 1–4.
- [6] Y. Miyamoto, J. M. Rios, A. G. Dentai, and S. Chandrasekhar, "Reduction of base-collector capacitance by undercutting the collector and sub-collector in GaInAs/InP DHBTs," *IEEE Electron Device Lett.*, vol. 17, pp. 97–99, Mar. 1996.
- [7] I. Schnyder, M. Rohner, E. Gini, D. Huber, C. Bergamaschi, and H. Jackel, "A laterally etched collector InP/InGaAs(P) DHBT process for high speed power applications," in *Proc. Int. Conf. Indium Phosphide and Related Materials*, 2000, pp. 477–480.

- [8] M. W. Dvorak, O. J. Pitts, S. P. Watkins, and C. R. Bolognesi, "Abrupt junction InP/GaAsSb/InP double heterojunction bipolar transistors with F_T as high as 250 GHz and $BV_{CEO} > 6V$," in *IEDM Tech. Dig.*, 2000, pp. 178–181.
- [9] E. Caffin, L. Bricard, J. L. Courant, L. S. How Kee Chun, B. Lescaut, A. M. Duchenois, M. Meghelli, J. L. Benchimol, and P. Launary, "Passivation of InP-based HBTs for high bit rate circuit applications," in *Proc. Int. Conf. Indium Phosphide and Related Materials*, 1997, pp. 637–640.
- [10] T. Oka, K. Hirata, K. Ouchi, H. Uchiyama, K. Mochizuki, and T. Nakamura, "Small-scaled InGaP/GaAs HBTs with WSi/Ti base electrode and buried SiO_2 ," *IEEE Trans. Electron Devices*, vol. 45, pp. 2276–2282, Nov. 1998.

Third-Order Intermodulation Reduction by Harmonic Injection in a TWT Amplifier

Michael Wirth, Aarti Singh, John Scharer, and John Booske

Abstract—A method for reducing the two-tone third-order intermodulation products arising from two carrier frequencies at 1.95 and 2.00 GHz is demonstrated in a traveling wave tube-distributed amplifier. The optimum amplitude and phase of an injected second harmonic and the resulting intermodulation suppression of up to 24.2 dB are examined for fundamental drive levels approaching saturation.

Index Terms—Harmonic injection, IM3, nonlinear distortion, traveling wave tube.

I. INTRODUCTION

When multiple carrier frequencies are amplified in a traveling wave tube (TWT) or other nonlinear amplifier, various order intermodulation products (IMPs) arise from the sum and difference of these frequencies. Certain IMPs are of concern since they lie close to the fundamental tones being amplified, thereby limiting the useful bandwidth of the amplifier. For example, in a simple excitation of f_1 and f_2 , the two-tone third-order intermodulation products (IM3s) arise from $2f_1 - f_2$ and $2f_2 - f_1$, whereas fifth-order intermodulation products (IM5s) with nearby frequencies arise from $3f_1 - 2f_2$ and $3f_2 - 2f_1$. The work described here injects an additional signal into a TWT at the frequency of the second harmonic of the upper fundamental drive tone (f_2). When this injected signal at $2f_2$ is of the proper phase and amplitude, a significant reduction in the upper IM3 ($2f_2 - f_1$) is observed.

This paper presents a detailed experimental examination of IM3 reduction using the harmonic injection technique in a TWT distributed amplifier. A recent study by Aitchison *et al.* [1] has demonstrated the effectiveness of this technique in narrowband, solid-state amplifiers at 835 and 880 MHz. They obtain substantial reduction in IM3 levels by both second harmonic and difference-frequency injection techniques. Work by Datta *et al.* [2] and Wöhlbier *et al.* [3] describe theoretical

Manuscript received November 20, 2001; revised March 6, 2002. This work was supported in part by United States Air Force Office of Scientific Research (AFOSR) Grant 49620-00-1-0088 and DUSD (S&T) under the Innovative Microwave Vacuum Electronics Multidisciplinary University Research Initiative (MURI) Program, managed by AFOSR Grant F49620-99-1-0297, and the University of Wisconsin, Madison. The review of this brief was arranged by Editor D. Goebel.

The authors are with the Department of Electrical and Computer Engineering, University of Wisconsin, Madison, WI 53706 USA (e-mail: scharer@cptc.wisc.edu).

Publisher Item Identifier S 0018-9383(02)04876-1.